Identifying scattering obstacles
by the construction of nonscattering waves [*]

D. Russell Luke [†] and Anthony J. Devaney[‡]

Abstract

There are many methods for identifying the shape and location of scatterers from far field data. We take the view that the connections between algorithms are more illuminating than their differences, particularly with regard to the Linear Sampling Method [7], the Point Source Method [26] and the MUSIC algorithm [11]. Using the first two techniques we show that, for a scatterer with Dirichlet boundary conditions, there is a nontrivial incident field that does not generate a scattered field. This incident field, written as an expansion of eigenfunctions of the far field operator, is used in the MUSIC algorithm to image the shape and location of the obstacle as those points z where the incident field is orthogonal to the far field pattern due to a point source located at z. This has two intriguing applications, one for inverse scattering and the other for signal design. Numerical examples demonstrate these ideas.

1 Introduction

The inverse scattering literature abounds with methods to determine the shape of scatterers from far field data. Of principal concern here are the MUSIC algorithm [11], the Linear Sampling Method [7], the Point Source Method [26] and the connections between these methods. The connection between the MUSIC algorithm and Kirsch's Factorization Method [17] has been detailed by Cheney [5] and Kirsch [18] for scattering from point-like inhomogeneities. More recent studies [1, 16, 12, 13] approach an application of the MUSIC algorithm to scatterers of some specified size, relative to the wavelength, and are based on the finite-dimensional multi-static response matrix for point-like scatterers. Our results complement those of Hazard and Ramdani [15], although they were concerned with the mathematical justification of the decomposition of time-reversal operator (DORT)

[†]Department of Mathematical Sciences, University of Delaware, Newark 19716-2553, USA. E-mail: `rluke@math.udel.edu`

[‡]Electrical and Computer Engineering, Northeastern University, Boston, MA 02115, USA. E-mail: `devaney@ece.neu.edu`

method [27]. The DORT method also relies on the asymptotic behavior of the time-reversal operator as the scatterers become small. Our goal here is to provide an analysis in the continuum of the inverse problem of determing geometric information about scatterers of arbitrary size and shape that are illuminated by fields of arbitrary frequency.

Our central result, Theorem 3.1, is built upon the Linear Sampling Method of Colton and Kirsch [7] and shows that, on the boundary of a scatterer with Dirichlet boundary conditions, there is a nontrivial incident field that has arbitrarily small far field pattern. With the help of the Point Source Method of Potthast [26] we show in Corollary 3.2 that such an incident field does not generate a scattered field. Theorem 3.5 combines these results as the foundation for a MUSIC algorithm [11] for determining the shape and location of an obstacle. The technique indicates intriguing possibilities for the construction of *nonscattering fields* that might be used to shield obstacles from interrogating waves.

To our knowledge the analysis presented here shows for the first time the feasibility of the MUSIC algorithm for determining the shape and location of Dirichlet obstacles without dependence on the size of the obstacle or the frequency of the incident field. The next section introduces our notation and the background for our main theoretical results presented in Section 3. Practical implementations of a MUSIC-type algorithm are discussed in Section 4. We illustrate the effectiveness of the algorithm with two examples presented in Section 5.

2   Scattering Background

We consider acoustic scattering of small-amplitude, monochromatic, time-harmonic waves from one or more impenetrable, sound-soft obstacles embedded in an isotropic homogeneous medium. The obstacles are identified by the domain $\Omega \subset \mathbb{R}^m$, $m = 2$ or 3. The domain Ω is assumed to be bounded with a simply connected exterior and C^2 boundary $\partial\Omega$ and the unit outward normal ν. The governing equation is the Helmholtz equation:

$$(1) \qquad\qquad \left(\triangle + k^2\right) v(x) = 0, \quad x \in \Omega^o \subset \mathbb{R}^m,$$

where $\triangle$ denotes the Laplacian, $k \geq 0$ is the wavenumber, $\Omega^o := \mathbb{R}^m \backslash \overline{\Omega}$ and the closure of the open exterior is denoted by the complement of Ω, that is Ω^c. The surface of the obstacle is assumed to be perfectly absorbing or *sound-soft*. This is modeled with Dirichlet boundary conditions: $v = f$ on $\partial\Omega$ where, f is continuous on $\partial\Omega$.

2.1   General Incident Fields

Let

$$(2) \qquad\qquad\qquad\qquad v = v^i + v^s$$

where the total field $v : \Omega^c \to \mathbb{C}$ solves (1) on Ω^o with boundary data

$$(3) \qquad\qquad v(x) := 0 \quad \text{for } x \in \partial\Omega.$$

The incident field $v^i : \mathbb{R}^m \to \mathbb{C}$ solves (1) on $\mathbb{R}^m$. The scattered field $v^s : \Omega^c \to \mathbb{C}$ solves (1) on Ω^o with boundary data

$$(4) \qquad\qquad v^s(x) = -v^i(x) \quad \text{for } x \in \partial\Omega$$

and

$$(5) \qquad\qquad r^{\frac{m-1}{2}} \left(\frac{\partial}{\partial r} - ik \right) v^s(x) \to 0, \;\; r = |x| \to \infty,$$

uniformly in all directions.

By Green's formula we can express the scattered field on Ω^o by the boundary integral

$$(6) \qquad\qquad v^s(x) = \int_{\partial\Omega} \left\{ \frac{\partial\Phi(x,y)}{\partial\nu(y)} v^s(y) - \Phi(x,y) \frac{\partial v^s}{\partial\nu}(y) \right\} ds(y),$$

where $x \in \Omega^o$ and $\Phi(x,y)$ is the outgoing free-space fundamental solution to (1), also referred to as Green's function. As $|x| \to \infty$ one can see that the scattered field has the behavior

$$(7) \qquad\qquad v^s(x) \;=\; \frac{e^{ik|x|}}{|x|^{\frac{(m-1)}{2}}} \left\{ v^\infty(\widehat{x}) + O\left(\frac{1}{|x|} \right) \right\}, \;\; |x| \to \infty,$$

where the function v^∞ is the far field pattern on the unit sphere $\mathbb{S} := \{ \widehat{x} \in \mathbb{R}^m \,|\, |\widehat{x}| = 1 \}$ given by

$$(8) \qquad\qquad v^\infty(\widehat{x}) = \beta \int_{\partial\Omega} \left(\frac{\partial e^{-ik\widehat{x}\cdot y}}{\partial\nu}(y) v^s(y) - e^{-ik\widehat{x}\cdot y} \frac{\partial v^s}{\partial\nu}(y) \right) ds(y)$$

for $\widehat{x} \in \mathbb{S}$ with

$$(9) \qquad\qquad \beta = \begin{cases} \frac{e^{i\frac{\pi}{4}}}{\sqrt{8\pi k}}, & m = 2 \\ \frac{1}{4\pi} & m = 3 \end{cases}, \quad k > 0.$$

We define next the Herglotz wave operator $\mathcal{H} : L^2(\mathbb{S}) \to H^1_{loc}(\mathbb{R}^m)$ by

$$(10) \qquad\qquad (\mathcal{H}g)(x) := \int_{\mathbb{S}} e^{-ik\widehat{\eta}\cdot x} g(-\widehat{\eta}) ds(\widehat{\eta}), \quad x \in \mathbb{R}^m.$$

The corresponding Herglotz wave function is denoted $v_g(x) := (\mathcal{H}g)(x)$. Here H^1 denotes the Sobolev space of order 1. The signs in our definition are not standard, but they are chosen to assure consistency between the directions of incident waves and measurement points on the far field sphere. The physical interpretation of the signs is more apparent in a limited aperture setting [20].

3

Lemma 2.1 (Herglotz wave functions) *Herglotz wave functions $v_g(x) := (\mathcal{H}g)(x)$ with $g \in L^2$ are dense with respect to the $H^1(\Omega)$-norm in the space of solutions to the Helmholtz equation.*

Proof. This is Theorem 2.3 of [10]. See also [9, Theorem 2.3]. $\qquad\square$

By Lemma 2.1 and the Trace Theorems for elliptic equations [23], we can construct the density g_z such that $v_{g_z}(x) \approx \Phi(x,z)$ and $\frac{\partial v_{g_z}}{\partial \nu}(x) \approx \frac{\partial \Phi(x,z)}{\partial \nu}$ on $\partial\Omega$ arbitrarily closely for $z \in \Omega^o$ with respect to the $H^{1/2}$- and $H^{-1/2}$-norms respectively. By (6) and (8), for $z \in \Omega^o$ we have

$$
\begin{aligned}
v^s(z) &= \int_{\partial\Omega} \left\{ \frac{\partial \Phi(z,y)}{\partial\nu(y)} v^s(y) - \Phi(z,y) \frac{\partial v^s}{\partial\nu}(y) \right\} ds(y), \\
&\approx \int_{\partial\Omega} \left\{ \frac{\partial v_{g_z}(y)}{\partial\nu(y)} v^s(y) - v_{g_z}(y) \frac{\partial v^s}{\partial\nu}(y) \right\} ds(y), \\
&= \int_{\mathbb{S}} \int_{\partial\Omega} \left\{ \frac{\partial e^{ik(-\widehat{x})\cdot y}}{\partial\nu(y)} v^s(y) - e^{ik(-\widehat{x})\cdot y} \frac{\partial v^s}{\partial\nu}(y) \right\} ds(y) g_z(-\widehat{x}) ds(\widehat{x}) \\
&= \frac{1}{\beta} \int_{\mathbb{S}} v^\infty(\widehat{x}) g_z(-\widehat{x}) ds(\widehat{x}).
\end{aligned}
$$

(11)

Note that the boundary of the scatterer is no longer involved in the expression for the scattered field. Moreover, the above approximation does not depend on the boundary condition. At each point $z \in \Omega^o$, by the correct choice of the density g_z, we can, in principle, reconstruct the scattered field. In the case of obstacles with Dirichlet boundary conditions, knowing the scattered field allows one to determine the shape and location of the scatterer as the zeros of the total field, or by constructing an indicator function for the scatterer via the eigenfunction expansion theorem [21]. The problem, however, is that the accuracy of this reconstruction depends on finding a density g that approximates the fundamental solution on the boundary of the scatterer, which we don't know! The Point Source Method is concerned mainly with strategies for constructing the density g (see, for example, [24, 25, 26, 20]). Note also that the density g must contain information about the *evanescent* fields in v^s since none of this information is present in the far field pattern v^∞.

2.2 Plane Wave Scattering

There are two ways to view the last integral in (11) that distinguish many numerical methods in inverse scattering. By the first interpretation the last integral in (11) is an integral operator with the far field pattern v^∞ as a kernel. By the second interpretation, the kernel of the operator is the density g and the operator acts on the far field data v^∞. These two different approaches are best illustrated by considering the case of scattering from incident plane waves

(12)
$$
u^i(x;\widehat{\eta}) := e^{ik(\widehat{\eta})\cdot x}
$$

where the incident field is parameterized by the direction of propagation $\widehat{\eta} \in \mathbb{S}$. The corresponding scattered field and far field patterns are denoted $u^s(x;\widehat{\eta})$ and $u^\infty(\widehat{x},\widehat{\eta})$.

4

When the scattering is from an incident plane wave with direction $\widehat{\eta}$, we define the *far field operator* $\mathcal{F} : L^2(\mathbb{S}) \to L^2(\mathbb{S})$

$$\tag{13} \mathcal{F}f(\widehat{x}) := \int_{\mathbb{S}} u^\infty(\widehat{x}, \widehat{\eta}) f(\widehat{\eta}) \ ds(\widehat{\eta}).$$

This operator corresponds to the view of (11) as an integral operator with the data u^∞ as the kernel. In this case (11) becomes

$$\tag{14} u^s(z; \widehat{\eta}) \approx \frac{1}{\beta} \int_{\mathbb{S}} u^\infty(\widehat{x}, \widehat{\eta}) g_z(-\widehat{x}) ds(\widehat{x}) = \frac{1}{\beta} \int_{\mathbb{S}} u^\infty(-\widehat{\eta}, -\widehat{x}) g_z(-\widehat{x}) ds(\widehat{x})$$

where the last equality follows from the reciprocity relation

$$\tag{15} u^\infty(\widehat{x}, \widehat{\eta}) = u^\infty(-\widehat{\eta}, -\widehat{x}).$$

The fact that $(\mathcal{F}g_z)(-\widehat{\eta}) \approx \beta u^s(z, \widehat{\eta})$ is a coincidence of having selected the correct function g_z to operate on.

By the second interpretation the last integral in (11) is an integral operator with the density g_z as a kernel: $\mathcal{A}_{g_z} : L^2(\mathbb{S}) \to \mathbb{X}(z)$

$$\tag{16} \mathcal{A}_{g_z} f(z) := \frac{1}{\beta} \int_{\mathbb{S}} g_z(\widehat{x}) f(\widehat{x}) \ ds(\widehat{x}).$$

Here we have left the image space $\mathbb{X}$ ambiguous because the dependence of the kernel of $\mathcal{A}_{g_z}$ on the points z is not specified. Acting on the far field pattern corresponding to an incident plane wave with direction $\widehat{\eta}$, the operator $\mathcal{A}_{g_z}$ can be seen to be a *backpropagation operator* that propagates the far field back to the scattered field at $z \in \Omega^o$. We will occupy ourselves mostly with the latter interpretation, but our principal tool will be the far field operator of the first interpretation.

Lemma 2.2 (far field operator) *The far field operator* $\mathcal{F} : L^2(\mathbb{S}) \to L^2(\mathbb{S})$ *is compact.* $\mathcal{F}$ *is injective with dense range if an only if there does not exist a Dirichlet eigenfunction for Ω which is a Herglotz wave function.*

Proof. Compactness follows from the fact that the kernel is continuous. For the remainder of the statement see [8, Corollary 3.18]. $\qquad\square$

The far field operator has a useful factorization in terms of a Herglotz wave function and the mapping of radiating solutions to the Helmholtz equation from the boundary data to the far field pattern, denoted by $\mathcal{B}$.

Lemma 2.3 ($\mathcal{B}$) *Assume that k^2 is not an eigenvalue of $-\triangle$ in Ω. The mapping of radiating solutions to the Helmholtz equation from the boundary data to the far field pattern, $\mathcal{B} : H^{1/2}(\partial\Omega) \to L^2(\mathbb{S})$, is a compact, injective bounded linear operator with dense range and $range(\mathcal{B}) = range((\mathcal{F}^*\mathcal{F})^{1/4})$ where $\mathcal{F}^*$ denotes the adjoint of the far field operator. Moreover, the far field pattern of the outgoing fundamental solution to the Helmholtz equation, $\Phi^\infty(\cdot; z)$, is in the range of $\mathcal{B}$ if and only if $z \in \Omega$.*

5

Proof. See [17, Theorem 3.6] and [17, Theorem 3.7]. See also [4]. $\qquad\square$

For any incident wave v^i restricted to $\partial\Omega$ we have $-\mathcal{B}v^i = v^\infty$ and in particular incident fields that can be written as superpositions of plane waves, $v^i = \mathcal{H}g$, yield the desired factorization

$$(17) \qquad\qquad -\mathcal{B}\mathcal{H}g = \mathcal{F}g.$$

We slightly abuse the notation since, by our definitions of $\mathcal{H}$ and v^i we need to include a Trace operator restricting them to the boundary $\partial\Omega$. This should be clear from the context.

3 Nonscattering Fields

The next theorem, modeled after the Linear Sampling Method of [4], shows that there is a nontrivial density $\widehat{g}$ that converges to the nullspace of the far field operator.

Theorem 3.1 (normalized Linear Sampling) *Let Ω be a domain with smooth boundary and assume that k^2 is not a Dirichlet eigenvalue for $-\triangle$ on Ω. If $z \in \Omega$ then for every $\epsilon > 0$ there exists a solution g_z to*

$$(18a) \qquad\qquad \|\mathcal{F}g_z(\cdot) + \Phi^\infty(\cdot;z)\|_{L^2(\mathbb{S})} < \epsilon$$

such that

$$(18b) \qquad \lim_{z\to\partial\Omega} \|\mathcal{F}\widehat{g}_z\|_{L^2(\mathbb{S})} = 0 \quad and \quad \lim_{z\to\partial\Omega} \left\| \mathcal{H}\widehat{g}_z - \frac{f_z}{\|g_z\|_{L^2(\mathbb{S})}} \right\|_{H^{1/2}(\partial\Omega)} = 0.$$

where

$$(18c) \qquad \widehat{g}_z := \frac{g_z}{\|g_z\|_{L^2(\mathbb{S})}} \quad and \quad f_z \quad solves \quad \mathcal{B}f_z(\cdot) = -\Phi^\infty(\cdot;z).$$

Proof. Our proof is modeled after that of [6, Theorem 2.2]. Since $-\Phi^\infty(\cdot;z) \in \text{range}(\mathcal{B})$, by Lemma 2.3 there is a solution f_z to

$$(19) \qquad\qquad \mathcal{B}f_z(\cdot) = \Phi^\infty(\cdot;z).$$

By Lemma 2.1 and the Trace Theorem [23], since k^2 is not a Dirichlet eigenvalue for the negative Laplacian on Ω, the Herglotz wave operator is injective with dense range in $H^{1/2}(\partial\Omega)$. Hence for any $\epsilon' > 0$ there is a solution $g_z \in L^2(\mathbb{S})$ to

$$(20) \qquad\qquad \|\mathcal{H}g_z - f_z\|_{H^{1/2}(\partial\Omega)} \leq \epsilon'$$

and hence

$$(21) \qquad\qquad \left\| \mathcal{H}\widehat{g}_z - \frac{f_z}{\|g_z\|_{L^2(\mathbb{S})}} \right\|_{H^{1/2}(\partial\Omega)} \leq \frac{\epsilon'}{\|g_z\|_{L^2(\mathbb{S})}}.$$

6

Then by the continuity of $\mathcal{B}$ and the factorization (17) we have

$$(22) \qquad \left\|\mathcal{B}\mathcal{H}\widehat{g}_z - \mathcal{B}\frac{f_z}{\|g_z\|_{L^2(\mathbb{S})}}\right\|_{H^{1/2}(\partial\Omega)} = \left\|-\mathcal{F}\widehat{g}_z(\cdot) + \frac{\Phi^\infty(\cdot;z)}{\|g_z\|_{L^2(\mathbb{S})}}\right\| \le \frac{\epsilon}{\|g_z\|_{L^2(\mathbb{S})}}$$

where ϵ' is small enough that $C\epsilon' < \epsilon$ for the constant C depending on $\mathcal{B}$. Now as $z \to \partial\Omega$ we have $f_z(x) \to -\Phi(x, z)$ for $x \in \partial\Omega$, hence $\|f_z\|_{H^{1/2}(\partial\Omega)} \to \infty$ as $z \to \partial\Omega$. Since f_z is approximated by $\mathcal{H}g_z$ it then follows that $\|\mathcal{H}g_z\|_{H^{1/2}(\partial\Omega)} \to \infty$ as $z \to \Omega$. Note also that $\|\mathcal{H}g_z\|_{H^{1/2}(\partial\Omega)} \le \|\mathcal{H}g_z\|_{H^1(\Omega)}$, so by the Cauchy-Schwarz inequality we have $\|g_z\|_{L^2(\mathbb{S})} \to \infty$ as $z \to \partial\Omega$. In light of (22) this yields

$$\lim_{z\to\partial\Omega}\left\|-\mathcal{F}\widehat{g}_z(\cdot) + \frac{\Phi^\infty(\cdot;z)}{\|g_z\|_{L^2(\mathbb{S})}}\right\| = \lim_{z\to\partial\Omega}\|\mathcal{F}\widehat{g}_z\| = 0$$

while by (21) we have

$$\lim_{z\to\partial\Omega}\left\|\mathcal{H}\widehat{g}_z - \frac{f_z}{\|g_z\|_{L^2(\mathbb{S})}}\right\|_{H^{1/2}(\partial\Omega)} = 0.$$

This competes the proof. $\qquad\qquad\qquad\qquad\qquad\qquad\qquad\qquad\qquad\qquad\qquad\qquad\qquad$ $\square$

Note that we make no statement about the behavior of $f_z/\|g_z\|_{L^2(\mathbb{S})}$ as $z \to \partial\Omega$, hence it is unclear from (18b) what the behavior of $\mathcal{H}g_z$ is in the limit as $z \to \partial\Omega$. It is an open problem to characterize the rate at which $\|g_z\| \to \infty$ and $\|f_z\| \to \infty$.

Since the far field pattern is zero if and only if there is no scattered field, the above theorem implies that the incident Herglotz wave function $\mathcal{H}\widehat{g}_z$ does not scatter in the limit as $z \to \partial\Omega$. That is,

Corollary 3.2 (nonscattering incident fields) *Let $\widehat{g}_z$ given by (18c) satisfy (18b) for g_z satisfying (18a). Then the scattered field, $v^s_{\widehat{g}_z}$, corresponding to the incident Herglotz wave function $v^i_{\widehat{g}_z} = \mathcal{H}\widehat{g}_z$ has the behavior*

$$\lim_{z\xrightarrow{\Omega}\partial\Omega} v^s_{\widehat{g}_z}(x) = 0 \quad for \quad x \in \Omega^o \quad while \quad \lim_{x\xrightarrow{\Omega^o}\partial\Omega}\lim_{z\xrightarrow{\Omega}\partial\Omega} v^i_{\widehat{g}_z}(x) = 0.$$

Here $\xrightarrow{\Omega}$ indicates that the limit is taken by points from within Ω.

Our proof relies on the backpropagation interpretation of (11) that is central to the Point Source Method.

Lemma 3.3 (Backpropagation) *Assume that k^2 is not a Dirichlet eigenvalue of $-\triangle$ on Ω and let $x \in \Omega^o$. Given any $\delta' > 0$, there exists an $\epsilon' > 0$ such that for all $p_x \in L^2(\mathbb{S})$ satisfying*

$$(23) \qquad \left\|\Phi(\cdot, x) - \mathcal{H}p_x(\cdot)\right\|_{H^{1/2}(\partial\Omega)} < \epsilon'$$

one has

(24)
$$\left| u^s(x, \widehat{\eta}) - (\mathcal{A}_{p_x} u^\infty)(x, \widehat{\eta}) \right| < \delta'$$

where $\mathcal{A}_{p_x}$ is defined by (16).

Proof. This is a special case of [26, Theorem 5.1.2]. See also [20, Theorem 1]. $\qquad\square$

Proof of Corollary 3.2 To show the first limit we construct a backpropagation operator $\mathcal{A}_{p_x}$ to approximate $v^s_{\widehat{g}_z}$. For $\delta' > 0$ and $x \in \Omega^o$, by Lemma 3.3 there is an $\epsilon' > 0$ such that $p_x \in L^2(\mathbb{S})$ satisfying (23) also satisfies (24). The existence of such a p_x follows from the denseness of the Herglotz wave operator. Next denote

(25)
$$v^\infty_{\widehat{g}_z} := \mathcal{F}\widehat{g}_z$$

where $\widehat{g}_z$ is the density in Theorem 3.1. By [8, Lemma 3.16] the scattered field corresponding to $v^\infty_{\widehat{g}_z}$ is

(26)
$$v^s_{\widehat{g}_z}(x) = \int_{\mathbb{S}} u^s(x; -\widehat{\eta})\widehat{g}_z(-\widehat{\eta}) \, ds(\widehat{\eta}),$$

hence by equation (16), (26) and the Cauchy-Schwarz inequality

$$\left| v^s_{\widehat{g}_z}(x) - (\mathcal{A}_{p_x} v^\infty_{\widehat{g}_z})(x) \right|$$
$$= \left| \int_{\mathbb{S}} u^s(x; -\widehat{\eta})\widehat{g}_z(-\widehat{\eta}) \, ds(\widehat{\eta}) - \frac{1}{\beta} \int_{\mathbb{S}} p_x(\widehat{y}) \left(\int_{\mathbb{S}} u^\infty(\widehat{y}; -\widehat{\eta})\widehat{g}_z(-\widehat{\eta}) \, ds(\widehat{\eta}) \right) ds(\widehat{y}) \right|$$
$$= \left| \int_{\mathbb{S}} \widehat{g}_z(-\widehat{\eta}) \left(u^s(x; -\widehat{\eta}) - \frac{1}{\beta} \int_{\mathbb{S}} p_x(\widehat{y}) u^\infty(\widehat{y}; -\widehat{\eta}) \, ds(\widehat{y}) \right) ds(\widehat{\eta}) \right|$$

(27)
$$< C\delta' \|\widehat{g}_z\|_{L^2(\mathbb{S})} = C\delta'$$

where C is the surface area of the unit sphere. For x and δ' fixed $\mathcal{A}_{p_x}$ is bounded and linear, independent of $\widehat{g}_z$, thus, since $\lim_{z \xrightarrow{\Omega} \partial\Omega} \|v^\infty_{\widehat{g}_z}\|_{L^2(\mathbb{S})} = 0$, it follows that $\lim_{z \xrightarrow{\Omega} \partial\Omega} |\mathcal{A}_{p_x} v^\infty_{\widehat{g}_z}(x)| = 0$. Hence by (27) and the triangle inequality,

(28)
$$\lim_{z \xrightarrow{\Omega} \partial\Omega} \left| v^s_{\widehat{g}_z}(x) - (\mathcal{A}_{p_x} v^\infty_{\widehat{g}_z})(x) \right| = \lim_{z \xrightarrow{\Omega} \partial\Omega} |v^s_{\widehat{g}_z}(x)| < C\delta'$$

for arbitrary $\delta' > 0$ which completes the proof to the first statement.

To see the corresponding incident field behavior, note that the total field $v^i_{\widehat{g}_z} + v^s_{\widehat{g}_z}$ is continuous and since Ω has Dirichlet boundary conditions

$$(v^i_{\widehat{g}_z} + v^s_{\widehat{g}_z})(x) = 0 \quad \text{for} \ \ x \in \partial\Omega.$$

8

Thus, given any $\epsilon'' > 0$ there is a $\rho > 0$ such that for all $z \in \Omega$ and $x \in \Omega^o$ with dist $(x, \Omega) < \rho$, we have

$$|v_{\widehat{g}_z}^i(x) + v_{\widehat{g}_z}^s(x)| < \frac{\epsilon''}{2}.$$

Now, since for each $x \in \Omega^o$ there is a $\widehat{g}_z$ such that $\lim_{z \xrightarrow{\Omega} \partial\Omega} |v_{\widehat{g}_z}^s(x)| = 0$, we have by the triangle inequality, $|v_{\widehat{g}_z}^i(x)| < \epsilon''$ for arbitrary $\epsilon'' > 0$ and x near enough to $\partial\Omega$. This completes the proof. $\square$

Remark 3.4 By Theorem 3.1, the fact that $\lim_{x \xrightarrow{\Omega^o} \partial\Omega} \lim_{z \xrightarrow{\Omega} \partial\Omega} v_{\widehat{g}_z}^i(x) = 0$ implies that the gradient of this field is the sole contribution to the $H^{1/2}$-norm on $\partial\Omega$. Also note that we have made no assumptions about the frequency or the size of the scatterers, other than to assume that the wavenumber is not a Dirichlet eigenvalue for the scatterer. $\square$

Following [15] we interpret the integral operator on the right hand side of (14) as a time-reversal operator for the multistatic data of an antenna array arranged on the aperture $\mathbb{S}$ emitting time-harmonic fields. A transducer located at $r\widehat{\eta}$ for $r \gg 1$ emits a spherically spreading field $\Phi(r\widehat{\eta}, x)$ which, in the region of the scatterer Ω is approximately the plane wave $u^i(x, -\widehat{\eta})$. The resulting scattered field is measured in the far field at the antenna element located at $r\widehat{x}$. The recorded data $u^\infty(\widehat{x}, -\widehat{\eta})$ is reversed, or backpropagated, in order to reconstruct the scattered field around the obstacle. This multistatic data array is thus the discrete realization of the far field operator $\mathcal{F}$. The connection between the MUSIC algorithm and Kirsch's factorization method for scattering from an inhomogeneous medium has been detailed in [5, 18]. We will have more to say about the discrete operator in Section 4.2 where we investigate the spatial resolution as a function of the far field sampling frequency and the number of incident fields.

Denote the singular system of $\mathcal{F}$ by $(\sigma_n, \xi_n, \psi_n)$ where

(29)
$$\mathcal{F}\xi_n = \sigma_n\psi_n, \quad \text{and} \quad \mathcal{F}^*\psi_n = \sigma_n\xi_n$$

with singular values $|\sigma_n| > |\sigma_m|$ for $m > n$, left and right singular functions ψ_n and ξ_n respectively. Then, by (14), for the correct g_z we have

$$\mathcal{F}^*u^s(z, \cdot) \approx \Psi\Sigma\Xi^*g_z.$$

where Ψ and Ξ are the singular operators corresponding to ψ_n and ξ_n respectively and Σ is a diagonal operator with the the the singular values σ_n on the diagonal.

By Lemma 2.2, $\mathcal{F}$ has at most a countable number of discrete eigenvalues with zero as the only possible cluster point. In fact, zero is an eigenvalue if and only if k^2 is an eigenvalue of the negative Laplacian on the interior of Ω with corresponding eigenfunction a Herglotz wave function. Such k, if they exist, form a discrete set [23]. Thus, the null space of $\mathcal{F}$ is almost always trivial, though the eigenvalues decay exponentially by the analyticity of the kernel of $\mathcal{F}$.

9

The MUSIC algorithm is based on the observation that the set of Green's functions

(30)
$$\Phi^\infty(\widehat{\eta}; z) := \lim_{r \to \infty} \Phi(r\widehat{\eta}, z) = \beta e^{ik(-\widehat{\eta}) \cdot z}$$

for z near $\partial\Omega$ and all $\widehat{\eta} \in \mathbb{S}$, are nearly orthogonal to the *noise subspace* of $\mathcal{F}$. We discuss what we mean by the noise subspace in more detail in the next section. In precise terms we have

Theorem 3.5 (MUSIC) *Let Ω be a domain with smooth boundary and assume that k^2 is not a Dirichlet eigenvalue for the negative Laplacian on Ω. Let $(\sigma_n, \xi_n, \psi_n)$, $n \in \mathbb{N}$, be the singular system for the far field operator $\mathcal{F}$ with $|\sigma_n| \leq |\sigma_m|$ for $n > m$. Given any $\gamma > 0$ there is a vector $a \in l^2$ with $\|a\|_2 = 1$ and $\rho > 0$ such that for any $x \in \Omega^o$ satisfying $\mathrm{dist}\,(x, \Omega) < \rho$ we have*

(31)
$$\sum_{n=1}^{\infty} |a_n \langle \xi_n, \Phi^\infty(\cdot; x) \rangle_{L^2(\mathbb{S})}| < \gamma.$$

Proof. Let g_z and $\widehat{g}_z$ satisfy (18a)–(18b). By Corollary 3.2, there are $\delta > 0$ and $\rho > 0$ such that

(32) $\quad |v_{\widehat{g}_z}^i(x)| < \gamma \quad$ whenever $\quad \mathrm{dist}\,(z, \partial\Omega) < \delta \quad (z \in \Omega) \quad$ and $\quad \mathrm{dist}\,(x, \Omega) < \rho \quad (x \in \Omega^o).$

The density $\widehat{g}_z$ can be written as a linear combination of the singular functions ξ_n [8, Theorem 4.8]:

(33)
$$\widehat{g}_z = \sum_{n=1}^{\infty} \widehat{a}_n \xi_n \quad \text{where} \quad \widehat{a}_n = \frac{1}{\sigma_n} (\widehat{G}_z, \psi_n) \quad \text{and} \quad \widehat{G}_z := \mathcal{F}\widehat{g}_z.$$

This and (32) yields

(34)
$$\left| \sum_n \widehat{a}_n \langle \xi_n, u^i(x, -\cdot) \rangle \right| < \gamma \quad \text{for } \mathrm{dist}\,(x, \Omega) < \rho.$$

Next, we construct a new density $\widetilde{g}_z$ from $\widehat{g}_z$ by rotating the coefficients $\widehat{a}_n$ in the complex plane in such a way that the sum corresponding to (34) is of the magnitudes of the individual terms. Define

(35) $\quad \widetilde{g}_z = \displaystyle\sum_{n=1}^{N} \widetilde{a}_n \xi_n \quad$ where $\quad \widetilde{a}_n := e^{i\theta_n} |\widehat{a}_n| \quad$ for $\quad \theta_n := -\arg(\langle \xi_n, u^i(x, -\cdot) \rangle).$

For this density $\|\mathcal{F}\widetilde{g}_z\| = \|\mathcal{F}\widehat{g}_z\| \to 0$ as $z \xrightarrow{\Omega} \partial\Omega$ and $\|\widetilde{g}_z\| = \|\widehat{g}_z\| \leq 1$, so by the same argument as in the proof of Corollary 3.2, the corresponding scattered and incident fields have the behavior

$$\lim_{z \xrightarrow{\Omega} \partial\Omega} v_{\widetilde{g}_z}^s(x) = 0 \text{ for } x \in \Omega^o \quad \text{and} \quad \lim_{x \xrightarrow{\Omega^o} \partial\Omega} \lim_{z \xrightarrow{\Omega} \partial\Omega} v_{\widetilde{g}_z}^i(x) = 0.$$

As in (32), given any $\gamma > 0$ there are $\delta > 0$ and $\rho > 0$ such that $|\sum_n \widetilde{a}_n \langle \xi_n(\cdot), u^i(x, -\cdot) \rangle| < \gamma$ whenever $\mathrm{dist}\,(z, \partial\Omega) < \delta \quad (z \in \Omega)$ and $\mathrm{dist}\,(x, \Omega) < \rho \quad (x \in \Omega^o)$. But by our construction of $\widetilde{a}_n$ the summands are all non-negative real numbers, that is

(36)
$$\sum_n |\widetilde{a}_n \langle \xi_n(\cdot), u^i(x, -\cdot) \rangle| < \gamma \quad \text{for } \mathrm{dist}\,(x, \Omega) < \rho.$$

10

Finally, recalling that $u^i(x, -\widehat{\eta}) = \frac{1}{\beta}\Phi^\infty(\widehat{\eta}; x)$, after normalization of the coefficients $\widetilde{a}_n$ the result (31) follows. $\qquad\qquad\qquad\qquad\qquad\qquad\qquad\qquad\qquad\qquad\qquad\qquad\qquad\qquad\qquad\qquad\qquad\quad$ $\square$

Remark 3.6 Inequality (34) alone could be used for imaging with the MUSIC methodology, however the contrast of the resulting images is not strong enough for adequate results. In other words, x need not be very close to Ω in order to satisfy (34), and the resulting image does not have a sharp cutoff near the boundary.

4 Practical Implementation

4.1 The MUSIC Algorithm

Theorem 3.1 only states that *there exists* a density $\widehat{g}_z$ that can be used to construct nonscattering incident fields, it does not, however, suggest *how* one might calculate such a density. Arens [3] has shown that for a sound soft scatterer as we have here a regularization strategy such as Tikhonov regularization or spectral cutoff gives rise to a density with the desired properties. In other words, if at a point $z \in \Omega$ we solve (18a) using Tikhonov or spectral cutoff regularization then the corresponding density $\widehat{g}_{\alpha,z}$ can be used to construct an incident field satisfying Corollary 3.2 in the limit as the regularization parameter $\alpha \to 0$. There are two reasons why this is impractical: firstly, we don't know where the scatterer lies, and secondly we don't know about the behavior of $\widehat{g}_z$ for points $z \in \Omega^o$. Note, however, that the location of point z in the computation of the density $\widehat{g}_z$ is arbitrary, so long as it is not in the exterior of Ω. This suggests that the orthogonality of $\widehat{g}_z$ with the fundamental solution far fields $\Phi^\infty(\cdot; x)$ expressed in (31) is a phenomenon more intimately tied to the spectrum of the far field operator $\mathcal{F}$ than to the particular density $\widehat{g}_z$. Indeed, as (18b) shows, the desired density is in the "noise space" of $\mathcal{F}$. Denote the noise subspace of $\mathcal{F}$ by $\mathcal{N}_\gamma$ corresponding to the span of the singular functions ξ_n with singular values $|\sigma_n| < \gamma$ for $n > N_\gamma$. In the numerical experiments detailed below we take $\widehat{g}$ to be simply a linear combination of the elements $\xi_n \in \mathcal{N}_\gamma$ for a large enough cutoff.

In the conventional MUSIC application one usually works with the MUSIC γ-pseudospectrum defined by

$$(37) \qquad \mathcal{P}(x) := \frac{1}{\sum_{n > N_\gamma} \left| a_n \langle \xi_n(\cdot), \Phi^\infty(\cdot; x) \rangle_{L^2(\mathbb{S})} \right|} \geq \frac{1}{\gamma}.$$

This is what is usually imaged as a function of x. Note that for $x \in \Omega^o$, we have $\mathcal{P}(x) \to \infty$ as $x \to \partial\Omega$, yielding the image of the support of the obstacle as the points where $\mathcal{P}(x)$ is large.

Our focus thus far has been on finding the location and shape of the scatterer, but the fact that the constructed incident field is arbitrarily small at the boundary of the scatterer opens the door to the construction of fields that *avoid* certain obstacles that one might like to protect, while targeting others. In other words, the constructed incident field $v^i_{\widehat{g}_z}$ effectively *does not scatter*. In order to

11

illustrate this point, in our numerical experiments, instead of the usual MUSIC implementation, we show the *inverse* of the γ-pseudospectrum.

4.2 Resolution Analysis

The analysis above is in the continuum. In any practical application one will sample the far field at a finite number of discrete points $\widehat{x}_i$ for a finite number of incident fields with direction $\widehat{\eta}_j$; that is, the far field operator $\mathcal{F}$ given by (13) is replaced with the discrete multistatic response matrix $F \in \mathbb{C}^{M \times N}$. In this section we apply sampling criteria derived from the physical optics approximation in order to estimate how many incident fields and far field measurements one needs in order to achieve a specified spatial resolution. Other approaches are presented in [2, 16].

The criteria we develop are based on the physical optics approximation which is valid for very large wavenumbers k. The technique discussed above is not dependent on the wavenumber. Indeed, it works especially well at small wavenumbers in the *resonance region* for the scatterer, that is where the wavelength is on the order of the scatterer. Our estimates for sampling rates are overestimates in the sense that the spatial resolution predicted from a particular sampling rate in the far field is not as fine as what is actually achieved. The analysis of this section thus provides lower bounds on the predicted spatial resolution from a given sampling rate.

To begin, we recall the physical optics, or Kirchhoff approximation. Our treatment is standard (see [8, 19]) with the exception that our derivation also holds in $\mathbb{R}^2$. For very large wavenumbers, that is, very small wavelengths relative to the curvature of the obstacle, the face upon which the incident field impinges is nearly planar. As such, we can then approximate the normal derivative of the scattered field by the normal derivative of the incident field. Define Ω_+ to be the illuminated side of the scattering domain $\Omega_+ := \{x \in \partial\Omega \mid \langle \nu(x), \widehat{\eta} \rangle < 0\}$. The shadow of the scattering domain, Ω_-, is defined as $\Omega_- := \partial\Omega \backslash \overline{\Omega_+}$. The physical optics approximation for the scattered field is written

$$(38) \qquad \frac{\partial u^s(x, \widehat{\eta})}{\partial \nu(x)} \approx \begin{cases} \frac{\partial u^i(x, \widehat{\eta})}{\partial \nu(x)}, & x \in \Omega_+ \\ -\frac{\partial u^i(x, \widehat{\eta})}{\partial \nu(x)}, & x \in \Omega_- \end{cases} \quad , \quad k \gg 0.$$

This leads to the physically intuitive approximation that the normal derivative of the total field is twice the normal derivative of the incident field on the illuminated side and zero on the shadow of the scatterer.

Together with the representation for the scattered field [8, Theorem 3.12]

$$(39) \qquad u^s(x, \widehat{\eta}) = -\int_{\partial\Omega} \Phi(x, y) \frac{\partial u(y, \widehat{\eta})}{\partial \nu(y)} ds(y)$$

for $x \in \Omega^o$, the Kirchhoff approximation yields

$$(40) \qquad u^s(x, \widehat{\eta}) \approx -2 \int_{\partial\Omega_+} \Phi(x, y) \frac{\partial}{\partial \nu(y)} u^i(y, \widehat{\eta}) \, ds(y),$$

and

$$(41) \qquad u^\infty(\widehat{x}, \widehat{\eta}) \approx -2\beta \int_{\partial\Omega_+} e^{-iky\cdot\widehat{x}} \frac{\partial}{\partial\nu(y)} u^i(y, \widehat{\eta}) \, ds(y) = -2ik\beta \int_{\partial\Omega_+} e^{iky\cdot(\widehat{\eta}-\widehat{x})} \widehat{\eta} \cdot \nu(y) \, ds(y).$$

Similarly, on the shadow region we have

$$(42) \qquad u^\infty(\widehat{x}, -\widehat{\eta}) \approx 2\beta \int_{\partial\Omega_-} e^{-iy\cdot\widehat{x}} \frac{\partial}{\partial\nu(y)} u^i(y, -\widehat{\eta}) \, ds(y) = 2ik\beta \int_{\partial\Omega_-} e^{-iky\cdot(\widehat{\eta}+\widehat{x})} \widehat{\eta} \cdot \nu(y) \, ds(y).$$

The Divergence Theorem together with (41)-(42) yields

$$
\begin{aligned}
u^\infty(\widehat{x}, \widehat{\eta}) + \overline{u^\infty(-\widehat{x}, -\widehat{\eta})} \quad &\approx -2ik\beta \int_{\partial\Omega} e^{iky\cdot(\widehat{\eta}-\widehat{x})} \widehat{\eta} \cdot \nu(y) ds(y) + R(\widehat{x}, \widehat{\eta}) \\
&= 2\beta k^2 (1 - \widehat{\eta}\cdot\widehat{x}) \int_\Omega e^{ikz\cdot(\widehat{\eta}-\widehat{x})} \, dz + R(\widehat{x}, \widehat{\eta}) \\
&= 2(2\pi)^{m/2} \beta k^2 (1 - \widehat{\eta}\cdot\widehat{x}) \widehat{\mathcal{X}_\Omega}(k(\widehat{x}-\widehat{\eta})) + R(\widehat{x}, \widehat{\eta})
\end{aligned}
$$
$$(43)$$

where $\widehat{\mathcal{X}_\Omega}$ is the Fourier transform on $\mathbb{R}^m (m = 2 \text{ or } 3)$ of the indicator function of the obstacle and

$$(44) \qquad R(\widehat{x}, \widehat{\eta}) = 4ik\,\mathrm{Im}(\beta) \int_{\partial\Omega_-} e^{iky\cdot(\widehat{\eta}-\widehat{x})} \widehat{\eta} \cdot \nu(y) ds(y)$$

In most discussions of the physical optics approximation (see, for example, [19]) the setting is $\mathbb{R}^3$ and here the remainder term does not appear since by (9) $\mathrm{Im}(\beta) = \mathrm{Im}(1/(4\pi)) = 0$. In $\mathbb{R}^2$, however, β is complex-valued which gives rise to the unusual remainder term in the calculations above.

The connection to the Fourier transform above allows us to estimate the sampling requirements for the scatterer via the Whittaker-Shannon Sampling Theorem. Our data, the far field pattern, is in the so-called Fourier or frequency domain of the scatterer. This data lies on circles in the Fourier domain of the scatterer centered at the point $-k\widehat{\eta}$ where $\widehat{\eta}$ is the direction of the incident field. This is depicted in Figure 1.

For our purposes it is not necessary to carry out a detailed sampling calculation for the geometry shown in Figure 1 – an estimate based on sampling on a rectangular grid suffices. Our discussion of the sampling theory is terse; interested readers are referred to [14] for more details. We consider a cubic lattice of samples of some smooth function φ on $\mathbb{R}^m$ defined by

$$(45) \qquad \varphi_s := \mathrm{comb}\left(\frac{x}{\Delta x}\right) \varphi(x)$$

where Δx is distance between the samples and comb (x) is the m-dimensional "comb" function

$$\mathrm{comb}\,(x) := \sum_{|n|=-\infty}^{\infty} \delta(x - n)$$

for n a multi-index depending on the dimension $m = 2$ or 3. By the Convolution Theorem, the Fourier spectrum of the sampled function is

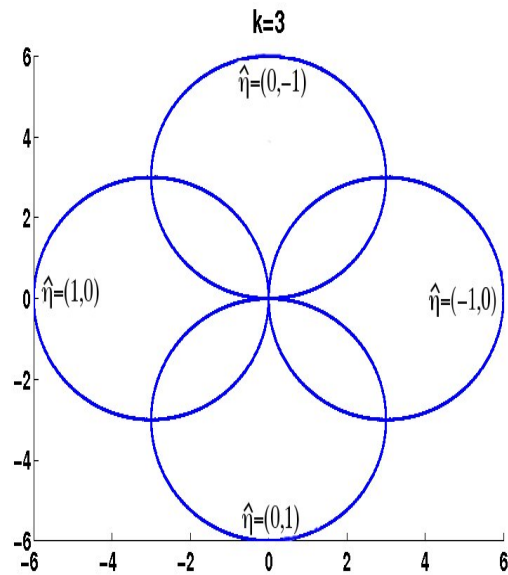$$\widehat{\varphi}_s(\xi) = (\Delta x)^m \,\mathrm{comb}\,(\Delta x\xi) * \widehat{\varphi}(\xi)$$

13

Figure 1: Sampling in the Fourier domain of the scatterer Ω corresponding to the geometry of the far field pattern in $\mathbb{R}^2$. The far field data is depicted here with wavenumber $k = 3$ at four incident fields with directions $\widehat{\eta} = (-1, 0), (0, -1), (1, 0)$ and $(0, 1)$. For each fixed $\widehat{\eta}$ the far field samples are depicted here as being a continuum on a full aperture $\mathbb{S}$.

where ξ is the Fourier dual variable to x and $*$ denotes convolution. It can be shown [14, Eq.(2–53)] that the sampled Fourier spectrum has the explicit representation

$$(46) \qquad \widehat{\varphi}_s(\xi) = \sum_{|n|=-\infty}^{\infty} \widehat{\varphi}\left(\xi - \frac{n}{\Delta x}\right)$$

where, again, n is a multi-index. If we assume that φ is bandlimited, then $\widehat{\varphi}$ has compact support. Suppose $\widehat{\varphi}$ is supported on the cube $\mathcal{R}$. If the sample spacing $1/\Delta x$ is large enough that for all $\xi \in \mathcal{R}$

$$\widehat{\varphi}\left(\xi - \frac{n}{\Delta x}\right) = \widehat{\varphi}_s(\xi)$$

then by (46) the sampled Fourier spectrum is just a periodic extension of the true Fourier spectrum, hence we can reconstruct φ exactly from the spectrum of the sampled function. If r is the length of the *smallest* cube that supports the spectrum of φ then the sampled spectrum will exactly represent the true spectrum as long as

$$\Delta x \leq \frac{1}{2r}.$$

When equality holds, the sampling is said to be at the Nyquist frequency. At the Nyquist frequency, we have the Whittaker-Shannon Sampling Theorem

$$(47) \qquad \varphi(x) = \sum_{|n|=-\infty}^{\infty} \varphi\left(\frac{n}{2r}\right) \text{sinc}\left(2r\left(x - \frac{n}{2r}\right)\right)$$

where sinc is the $m-$dimensional sinc function.

Let us suppose that the smallest feature of our scatterer is $1/M$ of the size of the illuminating wavelength. By the Whittaker-Shannon Sampling Theorem, a sampling rate of at least $1/(2M)$ in the physical domain represents a highest frequency component of M in each direction and thus $2M$ sample points on a Cartesian grid along each dimension in the Fourier domain. In Figure 1 we see that the "frequency domain" is covered by circles of radius k centered at $-k\widehat{\eta}$. The gaps in the frequency domain are determined by the smallest sampling rate with respect to either the direction of incidence $\widehat{\eta}$ or the far field samples $\widehat{x}$. Suppose that the far field is sampled at infinitesimal intervals and the directions of incidence are sampled at N points evenly distributed on $[-\pi, \pi]$. The largest gap in the frequency domain for this sampling geometry is bounded above by $2\pi k\sqrt{2}/N$. In order to achieve the same resolution as could be achieved by sampling on the Cartesian grid, N must be chosen so that

$$(48) \qquad \frac{2\pi\sqrt{2}}{N} \leq \frac{1}{M}$$

This yields a conservative lower bound on the sampling frequency N of the far field pattern and incident field directions needed to achieve a desired spatial resolution $1/M$ relative to the wavelength of the illuminating field. Since this analysis is based on the physical optics approximation, we expect these sampling requirements in the far field to be greater than what will actually be needed to resolve the scatterers. This is illustrated in the Section 5.

5 Examples

5.1 An infinite cylinder

As a first example we consider scattering from an infinite cylinder over which the field satisfies homogeneous Dirichlet conditions. While this example is didactic it has the advantage that the fields have explicit formulations. Taking advantage of radial symmetry, we parameterize directions on the unit sphere $\mathbb{S}$ by the angles α, where α_i is the direction of the incident field and α_0 is the observation point on the far field sphere. The incident and scattered fields can be represented in series of Bessel and Hankel functions, respectively. Let b be the cylinder radius, J_n and H_n^+ denote Bessel and Hankel functions of the first kind, respectively; then

$$(49) \qquad u^\infty(\alpha_0, \alpha_i) = -\sum_{n=-\infty}^{\infty} \frac{J_n(kb)}{H_n^+(kb)} e^{in(\alpha_i - \alpha_0)}.$$

It is easy to verify that the singular system $\{\psi_n, \xi_n, \sigma_n\}$ is, in this case, given by

$$\psi_n(\alpha_0) = \frac{1}{\sqrt{2\pi}} e^{\pm in\alpha_0}, \qquad \xi_n(\alpha_i) = \frac{e^{i\phi_n}}{\sqrt{2\pi}} e^{\pm in\alpha_i},$$

$$(50) \qquad \sigma_n = \left| \frac{J_n(kb)}{H_j(kb)} \right|$$

where $\phi_n = \mathrm{Arg}\,[J_n(kb)/H_n(kb)]$ and the plus sign gives one of the two singular vectors and the minus sign the second for each singular value σ_n.

For the density

$$g = \sum_{n}^{\infty} a_n \xi_n(\widehat{\eta})$$

we construct the incident Herglotz wave function
(51)

$$v_g^i(x) := \int_{\mathbb{S}} g(-\widehat{\eta}) u^i(x, -\widehat{\eta})\, ds(\widehat{\eta}) = \sum_{n}^{\infty} a_n v_n(x) \quad \text{where} \quad v_n(x) = \int_{\mathbb{S}} \xi_n(-\widehat{\eta}) u^i(x, -\widehat{\eta})\, ds(\widehat{\eta}).$$

By (29), the corresponding far field is given by

$$(52) \qquad v_g^\infty(\widehat{x}) := \int_{\mathbb{S}} g(-\widehat{\eta}) u^\infty(\widehat{x}, -\widehat{\eta})\, ds(\widehat{\eta}) = \sum_{n}^{\infty} a_n (\mathcal{F}\xi_n)(\widehat{x}) = \sum_{n}^{\infty} a_n \sigma_n \psi_n(\widehat{x}).$$

For this simple geometry, the incident and scattered fields have explicit formulations. The scattered field corresponding to v_g^i has the representation

$$(53) \qquad v_g^s = \sum_{n} a_n \sigma_n v_n^s(x) \quad \text{where} \quad v_n^s(x) = \int_{\mathbb{S}} \xi_n(-\widehat{\eta}) u^s(x, -\widehat{\eta}) ds(\widehat{\eta})$$

and u^s is the scattered field corresponding to an incident plane wave. In cylindrical polar coordinates, $x = (r, \theta)$, this simplifies to

$$(54) \qquad v_n^i(r, \theta) = \sqrt{2\pi} i^n J_n(kr) e^{\pm in\theta},$$

$$(55) \qquad v_n^s(r, \theta) = \sqrt{2\pi} e^{i\phi_n} i^n H_n^+(kr) e^{\pm in\theta}.$$

For details see [22].

For a Dirichlet obstacle, the total field is zero on the boundary, and, by Theorem 3.5, the incident field constructed from the finite collection of singular functions from N_γ to $\overline{N}$ is approximately zero:

$$\lim_{r \to b} \sum_{n=N_\gamma}^{\overline{N}} \left| J_n(kr) - \frac{J_n(kb)}{H_n(kb)} H_n(kr) \right|^2$$

$$(56) \qquad \approx \lim_{r \to b} \sum_{n=N_\gamma}^{\overline{N}} |J_n(kr)|^2 \approx 0$$

with $\overline{N} > N_\gamma$ and N_γ such that $\sigma_n < \gamma, \forall n > N_\gamma$.

We present a plot of the singular values $\sigma_n = |J_n(kb)/H_n(kb)|$ using unit wavelength ($k = 2\pi$) and cylinder radius $b = 35\lambda = 35$ in the top of figure 5.1. It is clear from this figure that the cutoff $N_\gamma \approx [kb] \approx 220$ where $[x]$ indicates the nearest integer approximation of x. In the bottom of the figure we show plots of the sums on the left and right-hand sides of (56) for the cases where $N_\gamma = [kb]$ and $N_\gamma = [kb] + 4$ and $\overline{N} = N_\gamma + 20$. The boundary of the cylinder is identified by where the incident field amplitude falls below a chosen cutoff. If this cutoff is chosen to be .02, then one would estimate the radius of the cylinder to be about 35 for the case $N_\gamma = 35$, while one would estimate the radius to be 36 for the case $N_\gamma = 39$. We obtained similar results for other choices of the cylinder radius b. We observed in our experiments that the sharpness of the zero of the constructed incident field at the boundary depends on the cut-off N_γ. The closer N_γ is to the optimal cut-off, kb, the higher the contrast.

5.2   Two ellipses

Our second example is of two ellipses in $\mathbb{R}^2$ shown in Figure 3. We use potential theoretic techniques to calculate the far field pattern for an incident plane wave. We introduce the acoustic single- and double-layer operators given respectively by

$$(S\varphi)(x) \quad := \quad 2 \int_{\partial\Omega} \varphi(y) \Phi(x, y) \, ds(y), \quad x \in \partial\Omega$$

$$(57) \qquad (K\varphi)(x) \quad := \quad 2 \int_{\partial\Omega} \varphi(y) \frac{\partial \Phi(x, y)}{\partial \nu(y)} \, ds(y), \quad x \in \partial\Omega,$$

where Φ is the two-dimensional outgoing free-space fundamental solution to the Helmholtz equation, a zeroth-order Hankel function of the first kind. It can be shown [8] that, if the potential φ satisfies
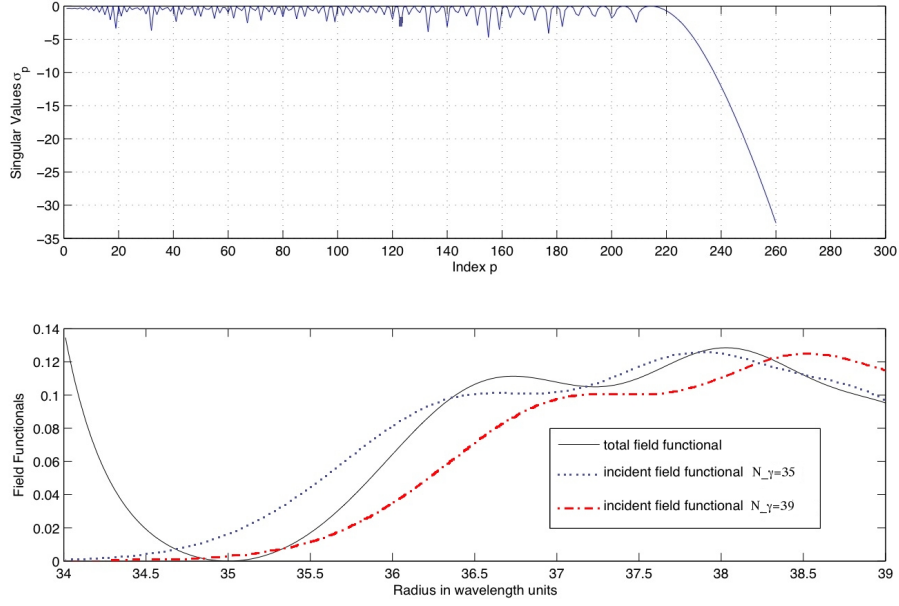
17

Figure 2: (Top) Plot of the singular values $\sigma_n = |J_n(kb)/H_n(kb)|$ with $k = 1$ for a cylinder having radius $b = 35$. (Bottom) Plots of the l.h.s. of (56) and the r.h.s. of this equation for $N_\gamma = 35$ and for $\overline{N} = N_\gamma + 20$ and for $b = 35$. Also shown is a plot of the r.h.s. of this equation for the case where $N_\gamma = 39$.

the integral equation

$$(58) \qquad\qquad (I + K - \mathrm{i}S)\varphi(\cdot; \widehat{\eta}) = -u^i(\cdot; \widehat{\eta}),$$

then the scattered and far fields are given by

$$(59\mathrm{a}) \qquad u^s(x, \widehat{\eta}) \;=\; \int_{\partial\Omega} \left(\frac{\partial \Phi(x,y)}{\partial \nu(y)} - \mathrm{i}\Phi(x,y) \right) \varphi(y; \widehat{\eta}) \, ds(y), \quad x \in \Omega^o$$

$$(59\mathrm{b}) \qquad u^\infty(\widehat{x}; \widehat{\eta}) \;=\; \beta \int_{\partial\Omega} \left(\frac{\partial e^{-\mathrm{i}\kappa\widehat{x}\cdot y}}{\partial \nu(y)} - \mathrm{i}e^{-\mathrm{i}\kappa\widehat{x}\cdot y} \right) \varphi(y; \widehat{\eta}) \, ds(y), \quad \widehat{x} \in \mathbb{S}.$$

We do not use a sophisticated quadrature rule to resolve the point source on the boundary. This introduces a numerical error of about 10% which has the advantage of introducing noise into our calculations, albeit systematic noise.

For $x \in \mathbb{R}^2$ fixed, we calculate the non-scattering incident field v_g^i shown in Figures 4–6 as

$$(60) \qquad\qquad v_g^i(x) = \sum_{n=N_\gamma}^{\overline{N}} |v_n^i(x)|$$

18

where v_n^i is given by (51). The corresponding scattered field is $v_g^s = \sum_{n=N_\gamma}^{\overline{N}} \sigma_n v_n^s(x)$ for v_n^s given by (53) with u^s is given by (59a).

To illustrate the resolution limits we sample the far field at $\overline{N} = 16$, 32, 64, and 128 points uniformly distributed over $\mathbb{S}$ with 16, 32, 64, and 128 incident field directions respectively, also uniformly distributed over $\mathbb{S}$. The wavenumber is $k = 3$ and the smaller ellipse has minor axes radius 0.25. By the resolution analysis of Section 4.2, our smallest physical feature is $1/6$ the illuminating wavelength, which according to (48) suggests that we need to sample the far field at $N \geq 2\pi\sqrt{2}(6) \approx 53$ points with more than 53 incident directions. This is more than is actually required, as an examination of the singular values of the far field operator show. In Figure 4 we show the magnitude of the constructed incident field for $\overline{N} = 32$ through 128 with $N_\gamma = \overline{N} - 12$. This value of N_γ was chosen based on the decay of the singular values shown in the left column of Figure 4. The singular values decay rapidly after the 7th singular value as predicted by the eventual exponential decay of the singular values of the far field operator. They flatten out, however, beyond the 20th singular value because of the error, or noise, in our calculation of the far field pattern. In other words, the 20th and higher singular vectors of the far field operator appear to be in the noise subspace. For a sampling rate of 32, we have $N_\gamma = \overline{N} - 12 = 20$ and our constructed incident field then consists of all available singular vectors in the noise subspace. For higher sampling rates of 64 and 128 there is not a significant difference in resolution when only the last 12 singular vectors are used.

The case $\overline{N} = 16$ shown in Figure 5 illustrates the reduction in resolution that results from constructing the incident field from singular vectors that are not in the noise subspace of $\mathcal{F}$. In Figure 5(b) we used the 12 smallest singular vectors to construct the incident field. As Figure 5(a) shows, most of these are still well within the signal subspace of the far field operator. With only the last 4 singular vectors we are able to achieve remarkably good results, as demonstrated in Figure 5(c).

To illustrate the relative robustness of the method with respect to the choice of the cutoff N_γ, so long as it is above the critical cutoff, in Figure 6 we show the constructed incident field with $N_\gamma = 25, 78$, and 124. The incident fields are not normalized in order to gauge the relative contrast between the images.

To verify that the constructed scattered field v_g^s, is indeed small outside the scatterer, we show in Figure 7 the computed scattered field using (53). The constructed scattered field is $O(10^{-13})$ around the scatterer and decays to zero rapidly away from the scatterer. The corresponding incident field, in contrast, is at least $O(10^{-4})$ on the exterior of the scatterer. This demonstrates Corollary 3.2.

6 Conclusion

Our main results, Theorem 3.1, Corollary 3.2 and Theorem 3.5, show that there is a density $\widehat{g}$ that approaches, nontrivially, the null space of the far field operator corresponding to some fixed, smooth
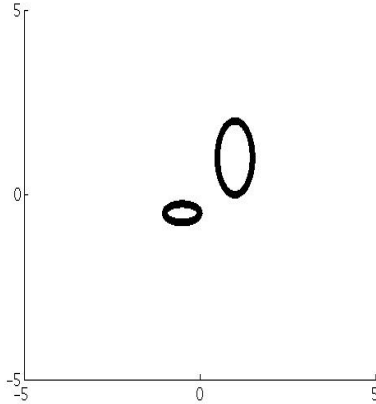
Figure 3: Sound-soft obstacles to be recovered.

scatterers. A superposition of plane waves weighted by such a density is a nonscattering incident field for these scatterers. The density can be constructed from the singular functions of the far field operator and the nonscattering phenomenon understood as the orthogonality of the singular functions to the far field pattern of a point source with sources located on the boundary of the scatterer. Since the image of this density acted upon by the far field operator vanishes, we arrive at the seemingly counterintuitive conclusion that it is the *noise* subspace of the far field operator that renders the shape and location of the obstacle, not the signal subspace. Our statement of Theorem 3.1 also raises unanswered questions about the rate of blow-up of the densities in the Linear Sampling Method.

The Point Source Method of Potthast [24, 25] rests on the approximation of the scattered field u^s by computing the correct density for the construction of a *backpropagation* operator (16). As already noted, constructing such a density is a nontrivial task since this requires some knowledge of the boundary of the scatterer which we assume is unknown. The Linear Sampling Method approaches the problem of finding the shape and location of the scatterer by looking for points where the fundamental solution far field pattern is not in the range of the far field operator, but still, one must solve an ill-posed linear integral equation at each point to be so tested in some computational domain. One of the disadvantages of the Linear Sampling methodology however is that, since it is not constructive, it provides very little information about numerical algorithms. Any numerical implementation will involve some sort of regularization strategy. The actual behavior of regularized solutions, or indeed any indication that a particular regularization strategy will deliver the desired behavior, remains open with the exception of the analysis of [3].

Our numerical experiments indicate, however, that particular details about implementing the Linear Sampling or Point Source Methods are somewhat beside the point: it is not necessary to create an approximate domain as with the Point Source Method, nor is it necessary to solve many ill-posed linear integral equations as in the Linear Sampling Method. We need only work with
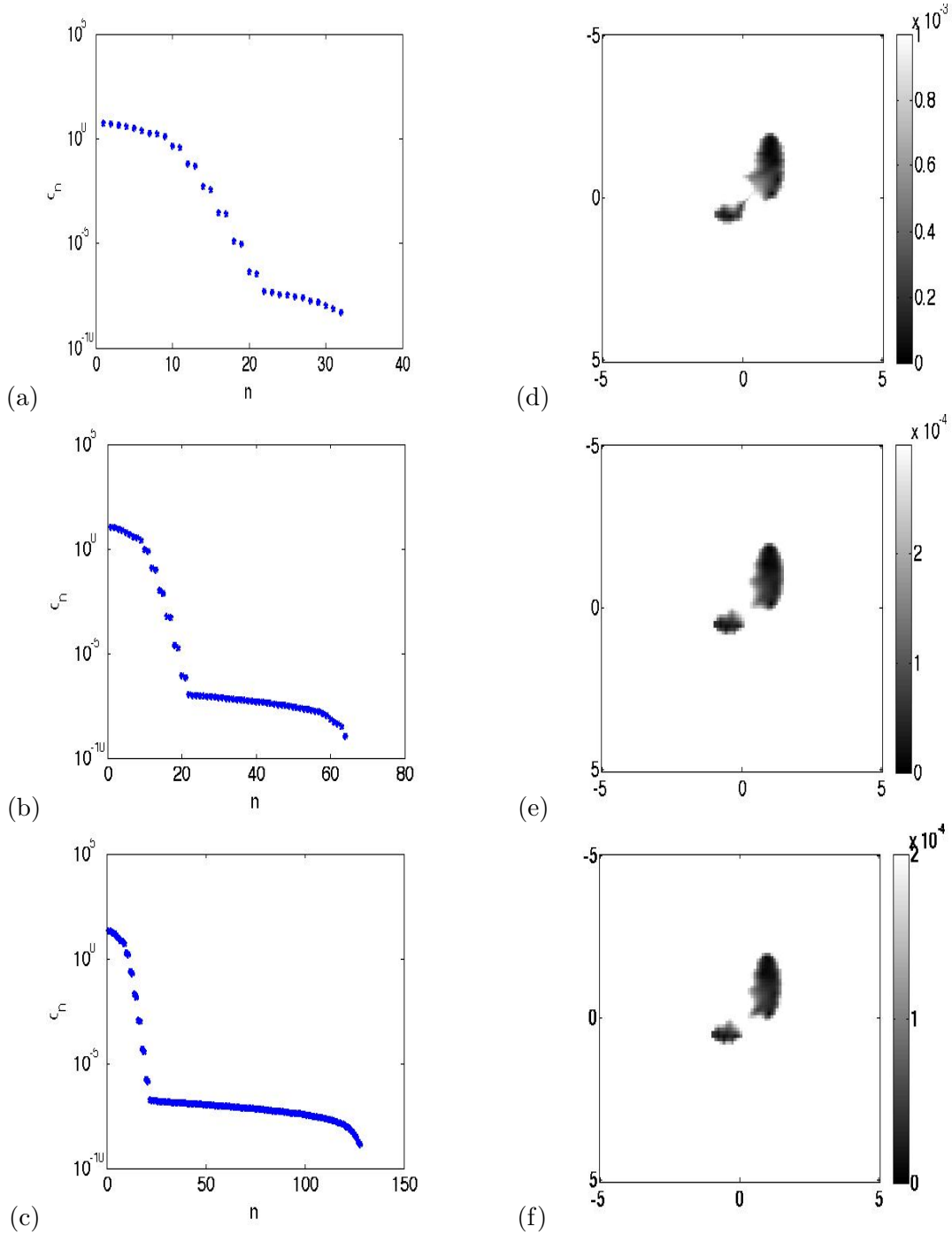
20

Figure 4: (a)-(c) Decay of the singular values of the multi-static response matrix for the far field sampled at 32 (a), 64 (b), and 128 (c) points for 32, 64 and 128 incident field directions respectively evenly distributed on $\mathbb{S}$. The far field pattern is calculated by (59b) to only about 10% accuracy which introduces noise into the experiment reflected in the lower plateau of the singular values. (d)-(f) The magnitude of the corresponding incident field $|v^i|$ calculated by (60) and (51) for the far field sampled at 32 (d), 64 (e), and 128 (f) points for 32, 64 and 128 incident field directions respectively evenly distributed on $\mathbb{S}$. The cutoff for each of these examples is $N_\gamma = \overline{N} - 12$ where $\overline{N} = 32, 64$ and 128 respectively.

(a)

(b)

(c)
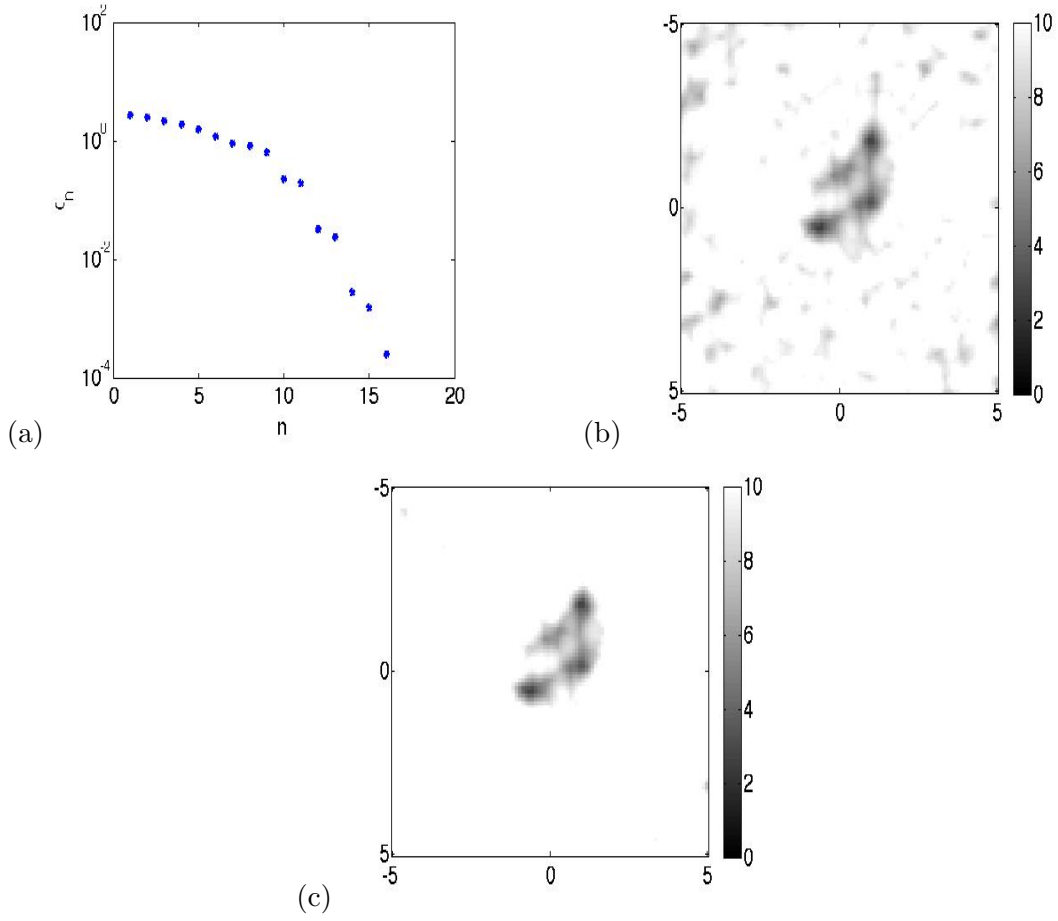
Figure 5: (a) Decay of the singular values of the multi-static response matrix for the far field sampled at 16 points for 16 incident field directions evenly distributed on $\mathbb{S}$. (b) The magnitude of the incident field $|v^i|$ calculated by (60) and (51) with cutoff $N_\gamma = 4$, $\overline{N} = 16$. (c) Incident field with $N_\gamma = 12$ and $\overline{N} = 16$.
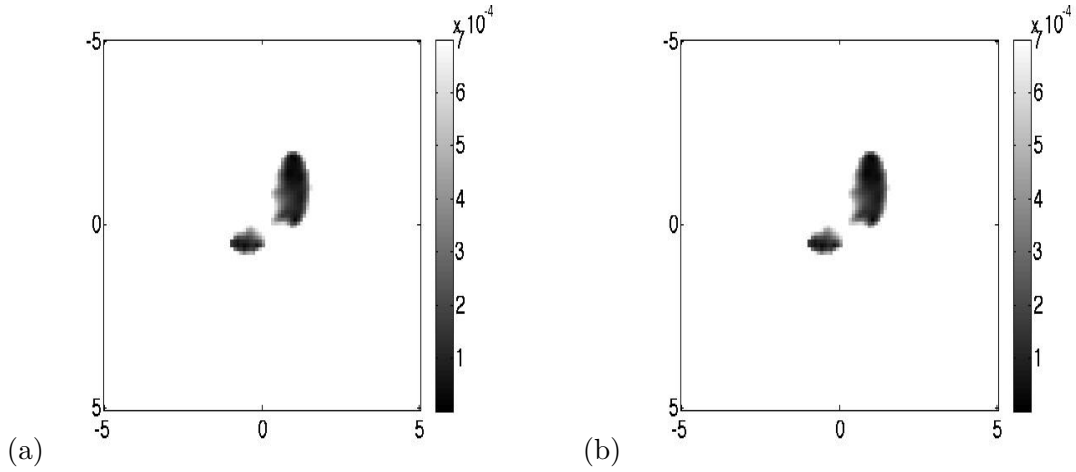
(a)   (b)

Figure 6: The magnitude of the incident field $|v^i|$ calculated by (60) and (51) for the far field sampled at 128 points with 128 incident field directions evenly distributed on $\mathbb{S}$. For each of these examples $\overline{N} = 128$ with cutoff $N_\gamma = 104$ (a), and $N_\gamma = 20$ (b).
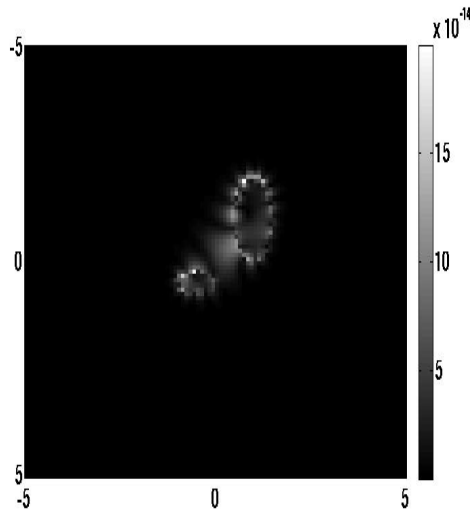

Figure 7: The magnitude of the scattered field calculated via (53) and (39) for the far field sampled at 128 points with 128 incident field directions evenly distributed on $\mathbb{S}$. Here $\overline{N} = 128$ and $N_\gamma = 116$.

incident plane waves and the known singular functions of the far field operator. This remains to be proved. We believe that the answer lies with a closer examination of the connections between Linear Sampling and the Factorization Method as detailed in [3]. This is the subject of future research.

These results have intriguing implications for inverse scattering and signal design. The method works very much like the Linear Sampling Method for inverse scattering in that the proposed incident field is constructed from the measured far field data and the scatterer is identified by those points in the domain where the incident field (and scattered field) are small. For signal design the method opens the door to the possibility of constructing signals that avoid certain known obstacles while irradiating others. Our application of the Linear Sampling Method to the MUSIC algorithm is novel and clarifies the connections between many different inverse scattering approaches.

Acknowledgments

References

[1] H. Ammari, E. Iakovleva, and D. Lesselier. Two numerical methods for recovering small inclusions from the scattering amplitude at a fixed frequency. *SIAM J. Sci. Comp.*, 27(1):130–158, 2005.

[2] R. Aramini, M. Brignone, and M Piana. The linear sampling method without sampling. *Inverse Problems*, 22(6), 2006.

[3] T. Arens. Why linear sampling works. *Inverse Problems*, 20:163–173, 2004.

[4] F. Cakoni and D. Colton. *Qualitative Methods in Inverse Scattering Theory*. Springer Verlag, Berlin, 2006.

[5] M. Cheney. The linear sampling method and the MUSIC algorithm. *Inverse Problems*, 17:591–595, 2001.

[6] D. Colton, H. Haddar, and M. Piana. The linear sampling method in inverse electromagnetic scattering theory. *Inverse Problems*, 19:S105–S137, 2003.

[7] D. Colton and A. Kirsch. A simple method for solving inverse scattering problems in the resonance region. *Inverse Problems*, 12(4):383–93, 1996.

[8] D. Colton and R. Kress. *Inverse Acoustic and Electromagnetic Scattering Theory*. Springer-Verlag, New York, 2nd edition, 1998.

[9] D. Colton and R. Kress. On the denseness of Herglotz wave functions and electromagnetic Herglotz pairs in Sobolev spaces. *Math. Meth. Appl. Sci*, 24:1289–1303, 2001.

[10] D. Colton and D. Sleeman. An approximation property of importance in inverse scattering theory. *Proc. of the Edinburgh Mathematical Society*, 44:449–454, 2001.

[11] A. J. Devaney. Time reversal imaging of obscured targets from multistatic data. *IEEE Trans. on Anten. Prop.*, 53(5):1600–1610, 2005.

[12] A. J. Devaney and E.A. Marengo. Nonradiating sources with connections to the adjoint problem. *Phys. Rev. E*, 70:037601, 2004.

[13] A. J. Devaney, E.A. Marengo, and F.K. Gruber. Time-reversal-based imaging and inverse scattering of multiply scattering point targets. *J. Acoust. Soc. Amer.*, 118:3129–3138, 2005.

[14] J. W. Goodman. *Introduction to Fourier Optics*. McGraw-Hill, 2nd edition, 1996.

[15] C. Hazard and K. Ramdani. Selective acoustic focusing using time-harmonic reversal mirrors. *SIAM J. Appl. Math.*, 64(3):1057–1076, 2004.

[16] S. Hou, K. Solna, and H. Zhao. A direct imaging algorithm for extended targets. *Inverse Problems*, 22(4):1151–1178, 2006.

[17] A. Kirsch. Characterization of the shape of a scattering obstacle using the spectral data of the far field operator. *Inverse Problems*, 14:1489–1512, 1998.

[18] A. Kirsch. The MUSIC algorithm and the factorization method in inverse scattering theory for inhomogeneous media. *Inverse Problems*, 18:1025–1040, 2001.

[19] R. Leis. Initial-boundary value and scattering problems in mathematical physics. In *Partial differential equations and calculus of variations*, Lecture Notes in Math., pages 23–60. Springer, Berlin, 1988.

[20] D. R. Luke. Multifrequency inverse obstacle scattering: the point source method and generalized filtered backprojeciton. *Math. and Computers in Simul.*, 66(4–5):297–314, 2004.

[21] D. R. Luke. Image synthesis for inverse obstacle scattering using the eigenfunction expansion theorem. *Computing*, 75(2–3):181–196, 2005.

[22] L. Mandel and E. Wolf. *Optical Coherence and Quantum Optics*. Cambridge University Press, Cambridge, 1995.

[23] W. McLean. *Strongly Elliptic Systems and Boundary Intgral Equations*. Cambridge University Press, Cambridge, 2000.

[24] R. Potthast. A fast new method to solve inverse scattering problems. *Inverse Problems*, 12:731–42, 1996.

[25] R. Potthast. A point-source method method for inverse acoustic and electromagnetic obstacle scattering problems. *IMA J. Appl. Math.*, 61:119–40, 1998.

[26] R. Potthast. *Point Sources and Multipoles in Inverse Scattering Theory.* Chapman & Hall, London, 2001.

[27] C. Prada and M. Fink. Eigenmodes of the time-reversal operator: A solution to selective focusing in multiple-target media. *Wave Motion*, 20:151–163, 1994.